*Kriosfera Zemli*, 2016, vol. XX, No. 4, pp. 84–92 **http://www.izdatgeo.ru**

# INSTABILITY OF CASING IN PERMAFROST PRODUCTION WELLS WITH A LATERAL SUPPORT FROM THAWING ICE-RICH SOIL

**J.B. Gorelik, P.V. Soldatov**

*Earth Cryosphere Institute, SB RAS, P/O box 1230, Tyumen, 625000, Russia; gorelik@ikz.ru*

Rzhanitsyn's general method for calculating the stability of an axially loaded column embedded into an elastic medium is used to estimate the critical load that leads to buckling of production well casing supported laterally by thawing ice-rich soil. In the suggested model, casing deforms within a thin layer of ice-rich soil subject to thawing, which resists elastically. The critical load depends on the thickness of the ice-rich layer, the stiffness of unfrozen soil, and the flexural rigidity of casing. The minimum critical load is a complex function of ice-rich thickness, while buckling can be either symmetrical or anti-symmetrical. Symmetrical buckling was detected instrumentally in an accidental well at the Yamburg gas-condensate field. Stronger three-string casing systems may help optimize well completion designs and reduce buckling risks in areas of deeply buried frozen soil.

*Frozen soil, thawing soil, well completion, casing, axial load, axial stability, buckling, symmetrical buckling, anti-symmetrical buckling*

## INTRODUCTION

Oil and gas wells in Arctic and Subarctic fields may experience an unusual effect like loss of axial stability (buckling): bending of casing strings over tens of meters within deep frozen intervals at the depths 200–250 m, which interferes with the operation and poses production risks. Note that the deformed casing remains laterally supported by the formation subject to thawing under heat released during drilling and poduction. Such an effect was observed at the Yamburg and Vankor gas fields and reported from some other high-latitude oil and gas fields (though not confirmed) but has received no explanation so far. Buckling happened also in production wells outside the permafrost zone, as a result of additional axial loads caused by loss of soil mineral component around wells [*Bratsev and Zhukov, 1965; Medvedsky, 1987*]. *Bratsev and Zhukov* [*1965*] mentioned cases of deformation in permafrost vertical mines when additional axial load arose during thawing. Note that most of deformation in mines occurs during first two or three years of operation, which coincides with the time of greatest thaw subsidence near production wells.

In a previous publication [*Gorelik et al., 2015*], we hypothesized that thawing soil around a well resists deformation and loads the well additionally in the axial direction (this load type known as negative friction is discussed in Section 3). Earlier *Medvedskiy* [*1987*] wrote about possible buckling in wells placed within deeply buried permafrost. To prove that possibility, he assumed that a thick ice layer melted at some depth and the overlying soil caved-in slightly above the former ice depth. The model used by *Medvedskiy* [*1987*] takes into account additional axial load from thawing soil but overlooks lateral support from the caved-in material. Furthermore, his solution eludes quality checking as it is fragmentary and many details remain unknown. Note also that freezing of wet soil in the cave (without regard to additional axial load) would hardly deform the casing because it does not produce significant pressure gradients across the hole axis [*Gorelik and Kolunin, 2002*]. However, such freezing can increase the pressure magnitude and cause buckling (which is actually observed during freeze-back). Another point to note is that sediments at these depths freeze up epigenetically, and the probability of cave-in during drilling is low because of compaction by overburden prior to freezing. On the other hand, the presence of thin ice-rich layers or even ground ice cannot be totally excluded due to specific processes associated with perennial freezing [*Dubikov, 2002; Gorelik, 2008*].

The general theory of axial stability loss (buckling) in columns with regard to lateral bearing pressure of the surrounding material was a subject of several earlier works [*Rzhanitsyn, 1955; Volmir, 1967; Timoshenko, 1971; Landau and Lifshits, 1987*]. The main problem is to proceed from the general theory to a specific system operated in certain conditions. In the case of a well, additional analysis is required for the choice of modeling strategy depending on the conditions of end support (whether the deformed casing segment has fixed or free ends); the method should be created to estimate the casing stability limits depending on the properties of frozen and thawing soil.

So far axial stability was estimated for surface casing bared upon thaw subsidence in the course of operation. Facts and overview of works on this kind of instability can be found in *Griguletsky* [*2013a,b*]. On the other hand, the problem remains unresolved for deeply buried permafrost, with implications for the operation safety of high-latitude production wells. The present study focuses on these and other aspects of the problem. Preliminary estimates show

the greatest impact on the stability of production wells from axial loads of thawing permafrost and casing weight. For this reason, our consideration is limited to axial load and related deformation. The effects of overpressure inside wells (or inside tubing), additional tubing tension, and other factors which may somehow affect the results, are neglected at this stage of research.

### 1. Choice of modeling strategy

In simulations for axial stability of wells, the real completion design is commonly simplified to a column of the respective size and mechanic properties of the casing material [*Birger and Mavlyutov, 1980; Vasilevskiy, 2002; Gasprom Company Standard, 2005*].

The strategy for buckling modeling depends on lithology and stratigraphy of frozen soil, its thawing patterns, and homogeneity along the section. We here consider formations that appear to be the most hazardous in terms of thawing impact on casing stability. Soils around petroleum wells are naturally heterogeneous: collapsible sand is intercalated with dense clay which has its structural strength and almost does not yield upon thawing. Such a clay layer, when unfrozen, can bear large loads and insulate the ground below from the subsiding overburden (including the backfilling material). This produces a zone of liquefied unconsolidated soil with low resistance to deformation (stiffness), for instance, due to high ice content between clay layers. Namely, inspection of accidental wells by experts from the *Gazpromdobycha Yamburg* company revealed ice-rich soil at the depths where the casing deformed, but no details of the section structure were reported. Note that core from a specially drilled permafrost hole 1 km far from the accidental well pad did not show high ice contents within those depths [*Gorelik et al., 2015*]. Thus, the section of frozen fine-grained sediments consists of dense clay layers which keep strong upon thawing (with the base of the upper layer at the depth $H$) and a collapsible soil layer of thickness $l$ between them, which is an analog of cave-in (suggested by Medvdedskiy) if its lateral strength is low.

This case can be modeled as follows. A cylindrical column has its ends fixed at the top and base of the weak soil layer. Total axial force applied to the column within the soil layer consists of the casing weight and negative friction within the segment from the ground surface to the depth $H$. Since the thickness $l$ is far smaller than $H$, the effect of casing weight and negative friction within the weak layer is vanishing. The length of the column exposed to deformation coincides with the thickness $l$. Within the interval between $H$ and $H + l$, soil resists deformation with its force proportional to the amount of buckling (Fig. 1). This case is discussed below in analysis of casing stability.

It is pertinent to cite some additional information on deformed wells in the Yambug and Vankor fields relevant for further consideration. Servicing at the Yamburg gas field showed deformation over ~40 m below 200 m. The radius of cave-in at this depth does not exceed 0.3 m and the deflection from the initial vertical direction is about 3 m (which means soil resistance). Similar inspection in the Vankor field revealed a 20 m long deformed segment below 170 m. The casing design is almost the same and the stiffness of thawing soil is unknown at both fields. For Yamburg, the compressibility of thawing soil is of the order of $10^{-8}$ Pa$^{-1}$, which approximately corresponds to a soil stiffness of $10^8$ Pa. However, it has been estimated for consolidated thaw soil (according to the existing methods), which requires correction in our case (see Section 3). Note also that ground ice

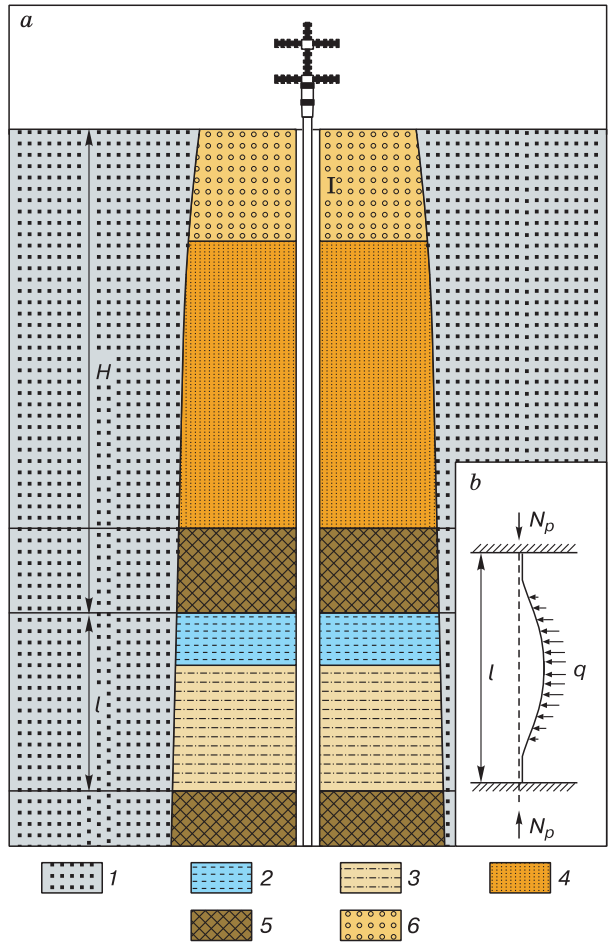


**Fig. 1. Sketch of a production well embedded in soil.**

*a*: vertical section of thaw annulus around a production well (I is casing string); *b*: model of loading ($q$ is lateral support from soil that resists buckling). *1* – frozen soil; *2* – water; *3* – poorly consolidated unfrozen soil; *4* – consolidated unfrozen soil; *5* – unfrozen dense clay; *6* – wellhead back-fill. See text for explanation.

was previously reported at the depth about 200 m, where deformation was obseved in the Vankor field [*Baulin et al., 1967*], but there is no exact data available on local geology and lithology at the well pad site.

## 2. Critical load

Buckling for a column with fixed ends embedded into an elastic medium was modeled by *Rzhanitsyn* [*1955*] in the general form. The bending equation of an elastically compressed column is

$$EJv^{\mathrm{IV}} + Pv^{\mathrm{II}} + bv = 0, \qquad (1)$$

where $E$ is the effective elasticity modulus of steel in casing strings and back-filling between them; $J$ is the area moment of inertia of the string cross section; $P$ is the total axial compressive load; $b$ is the stiffness of weak soil, Pa; $v$ is the deflection (function of its axial coordinate $x$; in some cases below we write $v(x)$ to highlight this dependence); the superscript at $v$ denotes the order of derivative along the coordinate $x$ of the column points.

Note that (1) implies proportionality (with the coefficient $b$) between the deflection and the elastic response of soil (stiffness) per column unit length [*Rzhanitsyn, 1955*]. Some authors use such relationship for bearing pressure of the medium instead of the linear force (e.g., [*Gorbunov-Posadov et al., 1984*]) and measure the stiffness $b^1$ in Pa/m. The same definition of stiffness is assumed in the Construction Norms and Regulations [*1986*]. The two approaches are equivalent and the coefficients are related as $b = db^1$, where $d$ is the column cross section size (diameter of the outer back-filled annulus). Below we use the coefficient $b$, while $b^1$, if necessary, is converted to $b$ via the specific diameter $d$.

The characteristic equation (which defines the general form of the solution) is a fourth-order algebraic equation with respect to $z$:

$$EJz^4 + Pz^2 + b = 0. \qquad (2)$$

The solution to (1) in the case of fixed ends is nonzero only provided that [*Rzhanitsyn, 1955*]

$$P > 2\sqrt{bEJ} > 0. \qquad (3)$$

All four roots of equation (2) are purely imaginary while their moduli are given by

$$z_1 = \sqrt{\frac{P}{2EJ} - \sqrt{\frac{P^2}{4E^2J^2} - \frac{b}{EJ}}},$$

$$z_2 = \sqrt{\frac{P}{2EJ} + \sqrt{\frac{P^2}{4E^2J^2} - \frac{b}{EJ}}}.$$

The general solution to (1) that defines the deformed shape of the column axis is

$$v(x) = C_1 \sin z_1x + C_2 \cos z_1x + C_3 \sin z_2x + C_4 \cos z_2x.$$

The unknown constants are found from the boundary conditions. For fixed column ends, the displacements and the strain first derivatives should be zero at the ends: $v(\pm l/2) = v^{\mathrm{I}}(\pm l/2) = 0$, with the origin of coordinates at the column midpoint and the length of the deformed column segment (equivalent to the weak soil thickness) denoted as $l$. The four linear algebraic equations with respect to four unknowns $C_1 - C_4$ obtained with any of these conditions are homogeneous, and the determinant is equated to zero in order to find nontrivial solutions. The determinant equation is

$$\left(-z_2 \cos\frac{z_1 l}{2}\sin\frac{z_2 l}{2} + z_1 \sin\frac{z_1 l}{2}\cos\frac{z_2 l}{2}\right)\times$$

$$\times\left(z_2 \sin\frac{z_1 l}{2}\cos\frac{z_2 l}{2} - z_1 \sin\frac{z_2 l}{2}\cos\frac{z_1 l}{2}\right) = 0.$$

The terms in braces refer to symmetrical and anti-symmetrical buckling. The first term corresponds to symmetrical buckling and provides additional relationship for defining its shape:

$$u_1 \mathrm{tg}\, u_1 = u_2 \mathrm{tg}\, u_2, \qquad (4)$$

while for anti-symmetrical buckling,

$$u_1 \mathrm{ctg}\, u_1 = u_2 \mathrm{ctg}\, u_2, \qquad (5)$$

where $u_1 = z_1(l/2)$, $u_2 = z_2(l/2)$. The critical load $N_p$, as a function of the length $l$, is defined by the parametric equation (taking into account (4) or (5)):

$$\frac{N_p}{\sqrt{bEJ}} = \frac{u_1}{u_2} + \frac{u_2}{u_1}; \qquad (6)$$

$$\frac{l}{\sqrt[4]{b/(EJ)}} = 2\sqrt{u_1u_2}. \qquad (7)$$

For example, $N_p(l)$ for symmetrical buckling can be obtained by successive exclusion of $u_1$ and $u_2$ from (4), (6), (7).

Details of the critical load calculations are not very clear from the cited publications and require additional explanation. Note that calculations of critical load in the theory of stability of column systems are preceded by estimation of the minimum column length at which the work of its material remains within the elasticity limit under critical load. It is generally straightforward because the critical load is expressed explicitly via the initial model parameters in simple cases (without elastic response of the medium), which is not our case though. Therefore, the applied and critical loads should be compared directly, after the critical load has been found, in order to check whether the material remains within the limits of elasticity:

$$\frac{N_p}{S} \le \sigma_e, \qquad (8)$$

where, for a two-string casing design, the sting cross section area is $S = 9.048 \cdot 10^{-3}$ m$^2$; $N_p$ is the critical load; $\sigma_e$ is the yield (elasticity limit) of the casing material $3.3 \cdot 10^8$ Pa (minimum for steel D used for the given casing).

For standard-size double casing consisting of a surface conduct pipe (245 × 11 mm) and production casing (168 × 12 mm), with the total flexural rigidity $EJ = 1.8 \cdot 10^7$ N·m$^2$, the calculations are as follows. Hereafter the subscripts *a* and *s* refer to anti-symmetric and symmetric solutions, respectively (e.g., $N_a$ or $N_s$ for $N_p$). In the case of anti-symmetrical buckling given by (5), *u* ctg *u* is an even function, and it is sufficient to consider the positive semi-axis of its domain. It zeroes at $\pi/2$, $3\pi/2$, $5\pi/2$, etc., has singularities at $\pi$, $2\pi$, $3\pi$ , etc., and is monotonous within the $(0, \pi)$ interval between two adjacent singularities.

Expressing $u_2$ via $u_1$ by (5) reduces the system of (6) and (7) to two one-parameter functions $N_a(u_1)$ and $l(u_1)$, and excluding the parameter $u_1$ leads to the sought function $N_a(l)$. However, the main problem is to pick the minimum critical load among multiple possible solutions to (5) or (4) which are ambiguous by periodicity of trigonometric functions. For instance, if the chosen values of $u_1$ belong to the monotonous interval from 0 to $\pi$, those of $u_2$ can be chosen from any monotonous interval, provided that $u_1 < u_2$, taking into account (3), and the number of solutions is infinite. Enumeration of the intervals of initial values is possible also for $u_1$. Thus, one has to choose the solutions that correspond to the minimum critical load for each specific *l*, which requires quite rigorous mathematical analysis of the problem and sidetracks the physical and engineering aspects of the issue. In this study, satisfactory solutions are chosen proceeding from natural requirements of continuity for $N_p(l)$, minimality of the critical load for the compared solutions, and monotony for the decreasing function $N_p(l)$.

We do not analyze all possible solutions (some are given below) but just outline the principle algorithm for the choice of the sought load value: $u_1$ runs successively through the monotonous intervals of *u* ctg *u* taking values from the least possible to some maximum depending on the specified interval of the column length, while $u_2$ (defined by (5)) is chosen from the next monotonous interval with regard to $u_1 < u_2$. Although the function in (5) has its singularities, thus found dependence $N_a(l)$ turns out to be continuous and corresponds to the minimum critical load at each *l*. Any other way of solving the problem (among those we tried) is inconsistent with at least one of the above conditions.

The variables $u_1$ and $u_2$ can be expressed via new variables $\alpha$ and $\beta$ as

$$u_1 = (2n+1)\frac{\pi}{2} + \alpha\,,\ |\alpha| \le \frac{\pi}{2}\,,\ u_2 = (2n+3)\frac{\pi}{2} + \beta, \quad (9)$$

$$|\beta| \le \frac{\pi}{2}\,,\ n = 0, 1, 2, \ldots,$$

where *n* is the number of the monotonous interval of *u* ctg *u*. Substituting (9) into (5) and using the cotangent conversion formulas, we obtain instead of (5):

$$\left((2n+1)\frac{\pi}{2} + \alpha\right)\mathrm{tg}\,\alpha = \left((2n+3)\frac{\pi}{2} + \beta\right)\mathrm{tg}\,\beta\,. \quad (10)$$

Calculations begin with numerical search of such $\beta(\alpha)$ value for each $\alpha$ from the interval specified in (9) that ensures the fulfillment of (10) at given *n* (starting from $n = 0$). See the curves for $n = 0$ and $n = 1$ in Fig. 2, *a*.

With the found function $\beta(\alpha)$, the variables $u_1$ and $u_2$ can be expressed as functions of a single parameter ($\alpha$). Then equations (6) and (7) are used to plot the functions $l(\alpha)$ and $N_a(\alpha)$, as in the example of Fig. 2, *b* for *l* as a function of $\alpha$ for two first monotonous intervals ($n = 0$ and $n = 1$) and $b = 6 \cdot 10^5$ Pa. Note that the value of $l(\alpha)$ in the end of the first monotonous interval ($n = 0$, $\alpha \to \pi/2$) is the same as in the beginning of the second interval ($n = 1$, $\alpha \to -\pi/2$). This ensures the continuity of $l(\alpha)$ across the interval boundaries (given the presence of a singularity in the cotangent, the function $l(\alpha)$ is sown at this point either with asymptotic relationships or by interpolation). The function value in the end of the second interval marks the upper bound of the length range (34.5 m in our case). If this value is insufficient for investigating the stability of the system, the third monotonous interval is included assuming $n = 2$ in (10). At each monotonous interval, one can find the function $\alpha(l)$ inverse to $l(\alpha)$ and substitute it into (6) to obtain the sought $N_a(l)$ for the chosen interval, for the entire range of the lengths (layer thicknesses) *l* with a sufficient number of successive intervals.

For the case of symmetrical buckling, the function $N_s(l)$ is found in the same way but using (4) instead of (5). Note however that the length ranges corresponding to the same *n* values are different for symmetrical and anti-symmetrical buckling (other

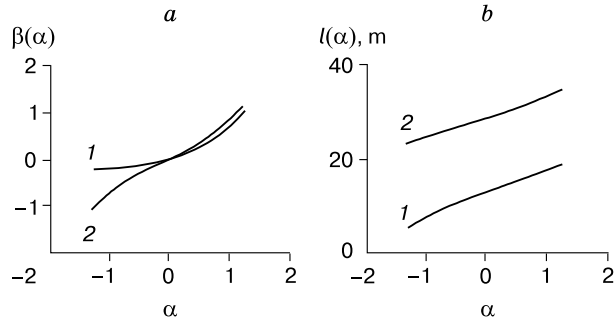


**Fig. 2. Behavior of model functions.**

*a*: parameter $\beta(\alpha)$ in anti-symmetrical case (*1* – $n = 0$; *2* – $n = 1$); *b*: length of deformed column segment in monotonous intervals (*1* – $n = 0$; *2* – $n = 1$).

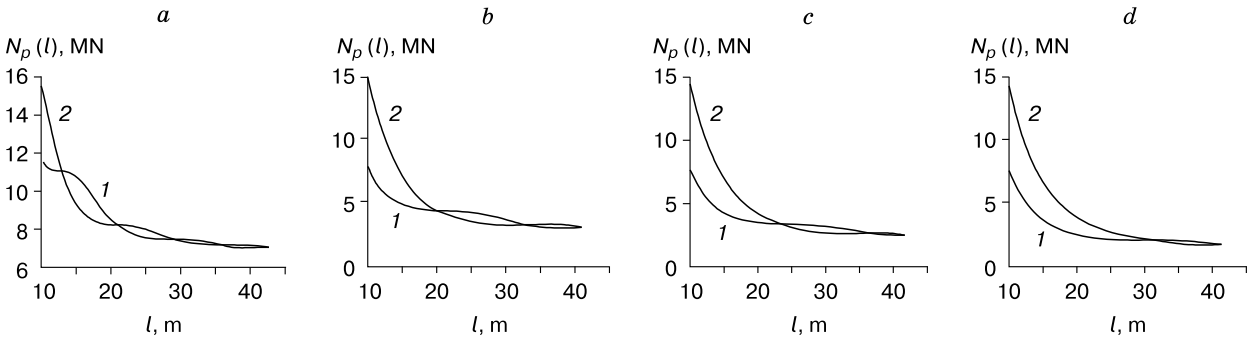


**Fig. 3. Behavior of critical load functions in cases of symmetrical and anti-symmetrical buckling: $N_s(l)$ (line *1*) and $N_a(l)$ (line *2*), respectively, as different soil stiffness coefficients:**

$b = 6 \cdot 10^5$ Pa (*a*), $b = 1 \cdot 10^5$ Pa (*b*), $b = 6 \cdot 10^4$ Pa (*c*), and $b = 2 \cdot 10^4$ Pa (*d*).

parameters being equal). Namely, the lengths shown in Fig. 2, *b*, are in the ranges $0 < l < 20.5$ m (at $n = 0$) and $20.5 \text{ m} < l < 35.9$ m (at $n = 1$) for anti-symmetrical buckling but $0 < l < 12.5$ m (at $n = 0$) and $12.5 \text{ m} < l < 28.3$ m (at $n = 1$) for the symmetrical case. This difference has bearing on the number of half-waves for the given lengths.

Figure 3 shows behavior of critical load for symmetrical $N_s(l)$ and anti-symmetrical $N_a(l)$ buckling within the lengths $10 \text{ m} < l < 42$ m for four values of soil stiffness: $b = 6 \cdot 10^5$; $1 \cdot 10^5$; $6 \cdot 10^4$; and $2 \cdot 10^4$ Pa. The minimum critical load for the given casing design (rigidity *EJ*) and soil properties (thickness *l* and stiffness *b*) is the principal target of the casing stability calculations.

The dependence of the minimum critical load on the length of the deformed segment (thickness of weak soil), in both symmetrical and anti-symmetrical cases, is quite complex, but its values are of the same order of magnitude in the two cases. This leads to alternation of the length ranges which intermittently correspond to the minimum critical load for symmetrical or anti-symmetrical buckling. This alternation is especially evident at high soil stiffness (Fig. 3, *a*). For short lengths (small thicknesses), the minimum critical load always corresponds to symmetrical buckling. In this range, the critical load decreases rapidly as the deformed segment becomes shorter (both for symmetrical and anti-symmetrical buckling). In the case of weaker soil, this range (corresponding to the minimum for symmetrical buckling) broadens gradually (Fig. 3): 13 m (Fig. 3, *a*), 19 m (Fig. 3, *b*), 22 m (Fig. 3, *c*), and 31 m (Fig. 3, *d*). At $b = 5 \cdot 10^3$ N/m$^2$, the upper bound reaches 37 m. Note also that the initial segment spans the whole range of our interest (until 42 m), where the minimum critical load corresponds only to symmetrical buckling, if (4) or (5) are solved for $u_2$ within an interval separated by another interval from the $u_1$ variation domain rather than within the interval next to $u_1$ (for this $2n + 5$ is used instead of $2n + 3$ in the right-hand sides of (9) and (10)). In that case, the minimum critical load always exceeds that in the solutions for adjacent intervals (Table 1).

Table 1. **Calculated critical loads (1 tf = $10^4$ N)**

| No. | *b*, Pa | $N_s/N_a$, tf | |
|---|---|---|---|
| | | $l = 20$ m | $l = 40$ m |
| 1 | $6 \cdot 10^5$ | 847/822 | 697/708 |
| 2 | $1 \cdot 10^5$ | 447/446 | 306/321 |
| 3 | $6 \cdot 10^4$ | 349/413 | 248/259 |
| 4 | $2 \cdot 10^4$ | 238/380 | 178/155 |
| 5 | $5 \cdot 10^3$ | 193/368 | 99/107 |
| 6* | $5 \cdot 10^3$ | 715/1008 | 196/274 |

* Calculated for every second interval: $2n + 5$ instead of $2n + 3$ in the right-hand side of (10).

Thus, due regard for the position of $u_1$ and $u_2$ in adjacent intervals is required in the search for the minimum critical load. Taking into account the above evidence of deformation from accidental wells, the target lengths (ice-rich layer thicknesses) are 20 and 40 m. The calculated critical loads for symmetrical and anti-symmetrical buckling at different soil stiffness coefficients (including the minimum $b = 5 \cdot 10^3$ Pa) are listed in Table 1, along with values based on solutions to (10) at every second interval (line 6), for comparison. The critical values for both lengths decrease monotonously as *b* decrease, for both symmetrical and anti-symmetrical buckling (except for the case of an intermediate interval of much higher loads between the $u_1$ and $u_2$).

At a 40 m thick ice-rich layer ($l = 40$ m), the minimum critical load corresponds to symmetrical buckling for all *b*, except $2 \cdot 10^4$ Pa (Table 1). However, symmetrical buckling with one half-wave, as in the Yamburg case (with the above limitations), is possible only at $b = 5 \cdot 10^3$ Pa, while two or more half-waves form at all other *b* values. Therefore, soil in the weak layer should have rather low Young modulus in our case (which can be estimated specially near the accidental well).

At a 20 m thick ice-rich layer ($l$ = 20 m), four values of soil stiffness from $6 \cdot 10^4$ Pa and lower correspond to symmetrical buckling (lines 3–6 in Table 1). For two first $b$ values, the minimum load corresponds to anti-symmetrical buckling (lines 1, 2 in Table 1). Note that all loads exceeding 300 tf violate the condition (8), and a more complex version of the deformation theory for the casing material is required [*Volmir, 1967; Belyaev, 1975; Birger and Mavlyutov, 1980; Rzhanitsyn, 1982*].

It is interesting to compare the obtained critical loads with the solution to the classical Euler buckling problem (in the absence of lateral support and hence elastic soil response: at $b = 0$), with the same model parameters of casing rigidity and length of the deformed column segment with either fixed or free ends. In the classical problem, the minimum critical load that causes symmetrical buckling with one half-wave to a column with fixed ends is given by [*Birger and Mavlyutov, 1980*]

$$N_s = \frac{4\pi^2 EJ}{l^2}.$$

The resulting loads for $l$ = 20 and 40 m are, respectively, $N_s$ = 177.5 and 44.4 tf (1 tf = $10^4$ N). Comparison with the symmetrical critical loads in Table 1 shows that lateral support from soil increases the load proportionally to soil stiffness. This is consistent with the physics of the problem: the greater the soil resistance to deformation, the greater the load leading to irreversible failure. The values $N_s$ = 177.5 and 44.4 tf can be considered as the lower bound of critical load, at the respective lengths $l$, when $b$ tends to zero.

The form of the new (bent) column axis for symmetrical buckling $v_s(x)$ is defined by (with dimensionless coordinates $2x/l \to x$):

$$v_s(x) = \frac{\cos\left(u_1(l)\cdot x\right)}{\cos\left(u_1(l)\right)} - \frac{\cos\left(u_2(l)\cdot x\right)}{\cos\left(u_2(l)\right)}.$$

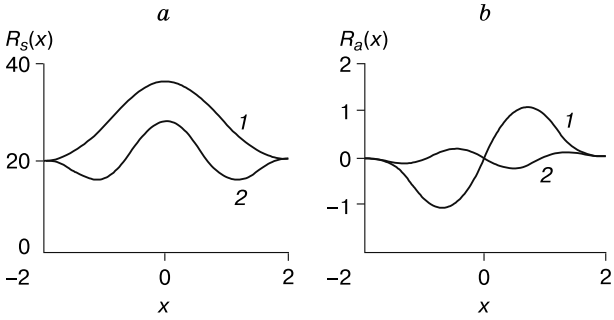


**Fig. 4. Symmetrical ($a$) and anti-symmetrical ($b$) buckling.**

*1* – $n$ = 0; *2* – $n$ = 1.

It is accurate to the constant term, assumed to be 1 (see below). The respective $v_a(x)$ for the anti-symmetrical case is

$$v_a(x) = \frac{\sin\left(u_1(l)\cdot x\right)}{\sin\left(u_1(l)\right)} - \frac{\sin\left(u_2(l)\cdot x\right)}{\sin\left(u_2(l)\right)},$$

where the functions $u_1(l)$ and $u_2(l)$ are found in the same way as $N_a(l)$ and $N_s(l)$.

The number of half-waves depends on the number $n$ of the interval where $u_1$ falls at the given $l$. The respective new stable buckling shapes for the symmetrical case (Fig. 4, $a$), at $n$ = 0 and 1, are: one half-wave at $n$ = 0 and three half-waves at $n$ = 1. The respective anti-symmetrical shapes (Fig. 4, $b$) are: two half-waves at $n$ = 0 and four half-waves at $n$ = 1. The minimum critical load that causes buckling of a column embedded into an elastic medium (soil), i.e., with lateral support, can produce more than one half-wave, unlike the classical Euler's model, without lateral support, where only one half-wave forms while more half-waves can appear only when the load exceeds the critical value. However, super-critical loading would rather lead to failure than to another half-wave [*Belyaev, 1975; Birger and Mavlyutov, 1980; Rzhanitsyn, 1982*].

Any kind of buckling poses risks to casing, but its specific shape is less important than the minimum critical load which is related directly with the casing design parameters. On the other hand, comparison of predicted and observed forms can help improving the calculation method. Note in this respect that the pre-

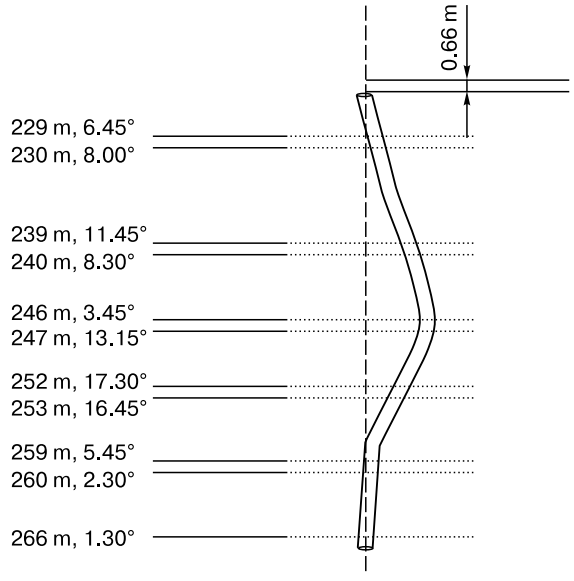


**Fig. 5. Buckling in an accidental well at Yamburg field.**

Numerals on the left show deflection (according to directional survey); 0.66 m above is wellhead subsidence. See text for explanation.

dicted buckling pattern with one half-wave, at $n = 0$ (Fig. 4, *a*), is similar to that observed at the Yamburg site (Fig. 5). Interpretation of directional survey data used to model the buckling shapes may be ambiguous and problematic. Specifically, directional surveys applied and interpreted in different times at the Yamburg field indicate either symmetrical or anti-symmetrical buckling of the same casing. Therefore, the pattern of Fig. 5 is rather illustrative and requires updating. Previously we [*Soldatov and Gorelik, 2015*] used alternative directional data, interpreted as anti-symmetrical buckling of the same well, when reported preliminary results of our study.

As for the Vankor site, there is no casing deformation data available. Generally, proceeding from the above results, either symmetrical or anti-symmetrical buckling can be expected at the minimum critical loads for the lengths $l = 20$ and 40 m, its magnitude depending on formation structure and the properties (stiffness) of thawing soil.

The suggested method for estimating critical load and shape of buckling, modified for practical uses, is quite straightforward and can be run automatically with some simple software (i.e., in *Mathcad*). For this, all solutions are preliminarily divided into symmetrical and anti-symmetrical subgroups, and monotonous intervals of the functions are selected within their determination domains, which facilitates the analysis. However, it is problematic to find easy solutions for specific conditions if a generalized approach is used initially.

The above inferences should be compared with real loads in order to formulate recommendations for specific wells.

### 3. Active vertical load

The origin and magnitude of load applied to well casing is important for analysis of its stability. The very existence of additional axial load on foundation piles from thawing soil was first noted by *Pchelintsev* [*1956*] who also estimated the magnitude of this load. The additional load from thawing soil on the surface elements of mines and oil or gas wells is obviously of the same nature. For piles it is calculated according to Construction Rules [*2012*], but its estimation in terms of the elasticity theory [*Kultikov, 1989*] has not reached much success, as the theoretical values have not been checked against observations. There is a method to account for this load using general equations of soil mechanics [*Tertsagi, 1961*], which one of us used to develop the respective design technology [*Gazprom Company Standard, 2005*], but the study has been incomplete. Numerical estimation of casing stability was applied to mines [*Guriyanov, 2000*], and similar approaches for wells and vertical mines were reported by *Bratsev and Zhukov* [*1965*] and *Khrustalev and Ershov* [*1999*]. These approaches and methods result from years-long research by a group from the Northern Division of the Gersevanov Research Institute of Bases and Underground Structures (NIIOSP) in Vorkuta: theoretical and experimental studies of processes around vertical mines and other structures upon frozen soil subject to thawing during operation. Although these methods have not been sufficiently grounded, they are used in design of mines in permafrost, and their results agree the best with observations at the operated sites. Therefore, the same methods are applicable to estimation of additional axial load on production well casing associated with permafrost thawing.

The total axial load on casing ($G$) consists of the weight of pipes $Q$ and negative friction $F$. The negative friction in a vertical mine of the radius $r$ and the height $H$, with the radius of thaw rocks around it $R$ is given by [*Bratsev and Zhukov, 1965*]

$$F = \pi r R \rho g H, \qquad (11)$$

where $\rho$ is the density of unfrozen soil; $g = 9.81$ m/c$^2$. Importantly, (11) includes the current thaw radius and, hence, records time dependence of the load. The thaw radius dependence of the load is distinctly traceable to about 4 m and then becomes weak (i.e., $R = 4$ m is used in (11) if the real radius is larger) [*Bratsev and Zhukov, 1965*]. It means that the effect of thaw radius is detectable only for a few years of operation.

Note, however, that the above calculations were for a single well, where unfrozen soil within the thaw radius is surrounded by frozen soil which acts as an additional stiff wall taking up a large part of load from thawing soil. In the case of multiple wells in pads with small spacing, the thaw zones may coalesce and the stiff frozen wall may fail. Then, the thaw radius in (11) should be meant as some effective value subject to change until half-spacing of wells. Growing thaw radius may influence negative friction and increase buckling risks. This explains why the Safety Rules [*2003*] postulate avoiding coalescence of thaw zones around neighboring wells.

The negative friction $F$ can be estimated to vary from 300–400 to 1000 tf, if the thaw radius in (11) is assumed to be $r = 0.2$ m (including the outer annulus), the $R$ range in the first years of operation is 2–4 m, the soil density is $\rho = 1500$–$2000$ kg/m$^3$, and $H = 200$ m. Of course, $F$ may be smaller (e.g., at a small thaw radius), but it is essential that the quoted values are possible at certain conditions.

For a 200 m long casing in a standard two-string design, the weight of pipes $Q$ (including back-fill material and production tree) is 79.4 tf (at the density of steel $\rho_s = 7800$ kg/m$^3$ and cement $\rho_c = 1800$ kg/m$^3$ and the linear weight of casing $q = 0.222$ tf per meter). Thus, the range of possible axial load variations, with regard to the casing weight, does not change much.

This actual load exceeds the estimated critical values and poses buckling risks to double casing if the

ice-rich layer is 20 and 40 m thick, at all soil stiffness coefficients used in our calculations (Fig. 3; Table 1). On the other hand, additional calculations show that the failure hazard can be reduced by using stronger casing (e.g., three-string design).

### 4. Estimating soil stiffness

The soil stiffness $b$ was assumed to be within $10^3$–$10^6$ Pa in the calculations of critical load in Section 2, without justification. This coefficient can be quite reliably estimated for soils with a relatively high Young modulus but is often hard to constrain for weak soils.

In its physics, the stiffness of soil (its elastic response to deformation) is close, in the linear approximation, to its Young modulus ($E$) or compressibility ($a$), an inverse of $E$. This makes basis for the theoretical estimation (e.g., [*Milyaev, 2007*]), but empirical methods proceeding from $E$ or $a$ determinations remain the most reliable [*Construction Norms and Regulations, 1986*]. The compressibility of thawing soil can be estimated in laboratory according to the State Standard [*2010*], provided that (i) melt water can be drained out of the soil sample; (ii) prior to thawing, the sample is loaded by a weight equivalent to the overburden at its *in situ* depth. Both conditions naturally work for soils and foundations within 10 m below the surface, but problems may arise in the case of large depths (100 m or more, as in test wells drilled at the Yamburg field). For instance, it is impossible to drain water out of thawing soil sandwiched between dense clay layers (aquicludes), where the soil remains poorly compacted and unconsolidated: the first condition fails. The other condition fails as well, because the conventional compressors cannot maintain the 2–4 MPa load that would correspond to overburden at the 100–200 m depths. Unfortunately, the inspection reports from the Yamburg test wells provide no explanation for this issue. In the absence of such loading, the coefficient $b$ becomes overestimated at the account of soil swelling [*Guidelines, 1973; Mazurov, 1975; Ershov, 1985*].

Thus, the methods for estimating soil stiffness for well casing stability in thawing permafrost remain poorly elaborated. Taking into account our results, the minimum stiffness (of the order of $10^7$ Pa) assumed according to the current building regulations [*Construction Norms and Regulations, 1986*] must be overestimated with respect to the real value. For this reason, the coefficients $b$ in the above calculations are two or three orders of magnitude lower than those for standard elastic soils.

## CONCLUSIONS

We have estimated critical loads required to cause buckling of laterally supported well casing and compared them with actual loads produced by negative friction during thawing of permafrost at specific oil and gas fields where emergency deformation of production wells was observed. The results allow the following inferences.

1. The magnitude of critical load on well casing in permafrost depends on thickness of ice-rich soil, stiffness of thawing soil, and strength (flexural rigidity) of the casing. The minimum critical load is a complex function of ice-rich thickness while well casing may experience either symmetrical or anti-symmetrical buckling with respect to the midpoint of the deformed segment. The number of buckling half-waves depends on the length of the deformed segment, other parameters being invariable, at least one half-wave at symmetrical buckling and two half-waves in the anti-symmetrical case. The deformation revealed instrumentally in accidental wells at the Yamburg field corresponds to symmetrical buckling.

2. Axial loads upon well casing are primarily due to negative friction produced by thawing soil and may range from a few hundreds to 1000 tf (depending on parameter values) and may exceed the minimum critical load leading to buckling (most often 100 to 500 tf, Table 1). Thus, production wells supported laterally by thawing soil around them are indeed prone to buckling, as the actual load often exceeds the critical value.

3. Deformation of this kind typically occurs at depths of 100 m or more, where negative friction is quite large (as it increases depthward), and is induced by thawing of ice-rich soil sandwiched between dense clay of high thawing strength. In some cases, cave-in between clay layers may act as such a weak layer.

4. Stronger casing, with three-string design, can reduce buckling risks in wells placed in deeply buried permafrost.

5. Design for placement of well pads in permafrost requires special attention to location and thickness of ice-rich soil. Methods for estimating deformation parameters of thawing soils at depths below 100 m need further development.

*We appreciate interest and support to our studies from directors of* Gazpromdobycha Yamburg *company. Special thanks go to V.F. Shtol, vice director general of Tyumen TyumenNIIGiprogaz Company, for useful advice.*

*The study was supported by grant SS-3929.2014.5 from the President of the Russian Federation to leading science schools and was carried out as part of Basic Research Program 11 of the Geoscience Department of the Russian Academy of Sciences.*

## References

Baulin, V.V., Belopukhova, E.B., Dubikov, G.I., Shmelev, L.M., 1967. Geocryological Conditions of the West Siberian Plain. Nauka, Moscow, 214 pp. (in Russian)

Belyaev, N.M., 1975. Strength of Materials. Nauka, Moscow, 608 pp. (in Russian)

Birger, I.A., Mavlyutov, R.R., 1980. Strength of Materials. Nauka, Moscow, 560 pp. (in Russian)

Bratsev, L.A., Zhukov, V.F. (Eds), 1965. Permafrost: Construction Theory and Practice. Nauka, Moscow, 188 pp. (in Russian)

Construction Norms and Regulations, 1986. Working Document SNiP 2.02.03-852.02.04-88. Pile Foundations. Gosstroyizdat, Moscow, 54 pp. (in Russian)

Construction Rules, 2012. Working Document SP 25.13330.2012. Basements and Foundations on Permafrost. Minregionrazvitiya, Moscow, 140 pp. (in Russian)

Dubikov, G.I., 2002. Composition and Cryostratigraphy of Permafrost in West Siberia. GEOS, Moscow, 246 pp. (in Russian)

Ershov, E.D. (Ed.), 1985. Stress and Strain in Freezing and Thawing Soils. Moscow University, Moscow, 165 pp. (in Russian)

Gazprom Company Standard, 2005. Working Document 16-2005. Casing Design of Production Wells with Regard for Permafrost Properties. IRC Gazprom, Moscow, 45 pp. (in Russian)

Gorbunov-Posadov, M.I., Malikova, T.A., Solomin, V.I., 1984. Design of Structures upon Elastic Foundations. Stroi'izdat, Moscow, 680 pp. (in Russian)

Gorelik, J.B., 2008. The mechanism of ice formation in connection with deformation of freezing layer, in: Proc. 9th Intern. Conf. on Permafrost. Fairbanks, Alaska, USA, pp. 535–540.

Gorelik, J.B., Kolunin, V.S., 2002. Physics and Modeling of Cryogenic Processes in the Lithosphere. Geo Publishers, Novosibirsk, 318 pp. (in Russian)

Gorelik, J.B., Soldatov, P.V., Seleznev, A.A., 2015. Thermal stability of frozen ground at sites of well clusters in the Yamburg gas-condensate field. Earth's Cyosphere (Kriosfera Zemli) XIX (1), 58–69.

Griguletsky, V.G., 2013a. Elastic stability of rectangular wellheads in production wells in high-latitude permafrost. Part 1. Stroitelstvo Neftyanykh i Gazovykh Skvazhin na Sushe i na More, No. 10, 7–14.

Griguletsky, V.G., 2013b. Elastic stability of rectangular wellheads in production wells in high-latitude permafrost. Part 2. Stroitelstvo Neftyanykh i Gazovykh Skvazhin na Sushe i na More, No. 11, 4–11.

Guidelines, 1973. Estimation of Physical, Thermal, and Mechanic Properties of Frozen Soils, Stroyizdat, Moscow, 191 pp. (in Russian)

Guriyanov, I.E., 2000. Operation of super-mine constructions in the central Siberian craton. Kriosfera Zemli IV (3), 42–48.

Khrustalev, L.N., Ershov, E.D. (Eds), 1999. Fundamentals of Geocryology. Part 5. Engineering Geocryology. Moscow University, Moscow, 518 pp. (in Russian)

Kultikov, A.M., 1989. Estimates of loads on casing at thawing of soils around wells in a cluster, in: Engineering-Geocryological Conditions of Construction, Nauka, Novosibirsk, pp. 88–96.

Landau, L.D., Lifshits, E.M., 1987. Theoretical Physics. Book VII. Theory of Elasticity. Nauka, Moscow, 248 pp. (in Russian)

Mazurov, G.P., 1975. Mechanics of Frozen Soils. Stroyizdat, Leningrad, 216 pp. (in Russian)

Medvedskiy, R.I., 1987. Construction and Operation of Petroleum Wells in Permafrost. Nedra, Moscow, 232 pp. (in Russian)

Milyaev, A.S., 2007. Estimation of soil stiffness in design of constructions with a circular cross section in an elastic medium. Izv. Vuzov. Lesnoi Zhurnal, No. 1, 67–74.

Pchelintsev, A.M., 1956. Lateral shear stress on basement due to ground thawing, in: Fundamentals of the Permafrost Theory. Izd. AN SSSR, Moscow, Issue 3, pp. 163–166. (in Russian)

Rzhanitsyn, A.R., 1955. Equilibrium Stability of Elastic Systems. Gostekhteoretizdat, Moscow, 475 pp. (in Russian)

Rzhanitsyn, A.R., 1982. Construction Engineering. Vysshaya Shkola, Moscow, 400 pp. (in Russian)

Soldatov, P.V., Gorelik, J.B., 2015. Buckling of well casing in permafrost, in: Arctic and Subarctic: Mosaic, Contrasting, and Variability of the Cryosphere. Proc. Intern. Conf. Tyumen, 2–5 July 2015, Epokha, Tyumen, pp. 361–367. (in Russian)

Safety Rules, 2003. Safety Rules 08-624-03 in Petroleum Production. Gosgortekhnadzor RF, Moscow, 168 pp. (in Russian)

State Standard, 2010. Working Document GOST 12248-2010. Soils: Methods for Laboratory Estimation of Soil Strength and Compliance. MNTKS, Moscow, 156 pp. (in Russian)

Tertsagi, K., 1961. Theory of Soil Mechanics. Gosstroyizdat, Moscow, 508 pp. (in Russian)

Timoshenko, S.P., 1971. Stability of Columns, Plates, and Shells. Nauka, Moscow, 808 pp. (in Russian)

Vasilevskiy, V.V., 2002. Improving Operation Stability of Gas and Oil Wells in Permafrost. Candidate Thesis (Engineering), Moscow, 163 pp. (in Russian)

Volmir, A.S., 1967. Stability of Deformable Systems. Nauka, Moscow, 984 pp. (in Russian)

*Received June 18, 2015*

This is especially the case for permafrost landscapes, where melting of excess ground ice and subsequent subsidence affect lateral processes which can substantially alter soil conditions and fluxes of heat, water and carbon to the atmosphere. Here we demonstrate how dynamically changing microtopography and related lateral fluxes of snow, water and heat can be represented with a tiling approach suitable for implementation in large-scale models, and investigate which of these lateral processes are important to reproduce observed landscape evolution. In the multiple well design cases, the permafrost thaw can also introduce lateral formation movements which are considered important in terms of their increased potential for developing casing buckling and shear deformations. Figure 3 shows a schematic representation of the casing deformation analysis model. The following considerations are included in the casing deformation analysis and design assessment: ï‚· The casing model starts at the surface level, where relative movement between casing and formation is permitted; and ends at a depth where the soil movements derived from soil deformation â€˜Ice-richâ€™ permafrost contains ice in excess of the soil pore spaces and is subject to settling on thawing. Formation and Thawing. Repeated glaciations over the last million years or so have caused sea level changes of 100 m or more (Figure 2). When sea levels were low, the shallow continental shelves in polar regions that were not covered by ice sheets were exposed to low mean annual air temperatures (typically !10 to !253C).Â  Thawed sub-sea permafrost is often separated from ice-bonded permafrost by a transition layer of ice-bearing permafrost. The thickness of the ice-bearing layer can be small, leading to a relatively sharp (centimeters scale) phase boundary, or large, leading to a diffuse boundary (meters scale). When the permafrost thaws, the ice wedge melts and the enclosing and overlying sediments collapse into the trough. Typically, composite wedges are filled with material very similar in structure and texture to sands in a typical fissure of primary filling (i.e., sand wedge). However, there may be inclusions of material from the fissure walls and some distortion of the adjacent sediments bordering the wedge, reflecting the presence of ice in the original fill material. REFERENCES: Black and Berg, 1966; Gozdzik, 1973; French, 1976; Washburn, 1979.Â  COMMENT: In frozen soils, creep deformations are due mainly to the creep of pore ice and the migration of unfrozen pore water. In ice-saturated frozen soils, most creep deformations are distortional with little or no volume change.